

Replacement of the Axial Histidine Ligand with Imidazole in Cytochrome *c* Peroxidase. 2. Effects on Heme Coordination and Function[†]

Judy Hirst,^{‡,§} Sheri K. Wilcox,^{‡,||} Jingyuan Ai,[⊥] Pierre Moënne-Loccoz,[⊥] Thomas M. Loehr,[⊥] and David B. Goodin^{*,‡}

Department of Molecular Biology, MB8, The Scripps Research Institute, 10550 North Torrey Pines Road, La Jolla, California 92037, and Department of Biochemistry and Molecular Biology, Oregon Graduate Institute of Science and Technology, 20000 NW Walker Road, Beaverton, Oregon 97006-8921

Received September 5, 2000; Revised Manuscript Received November 20, 2000

ABSTRACT: The inability of imidazole to complement function in the axial histidine deletion mutant, H175G, of yeast cytochrome *c* peroxidase has been an intriguing but unresolved issue that impacts our understanding of the role of axial ligands in heme catalysis. Here we report the functional and spectroscopic properties of H175G and of its complexes with imidazole. Combined with the crystal structures for these complexes, the data provide a detailed and consistent account of the modes of Im binding in the H175G cavity and their dependence on buffer and pH. UV–vis, EPR, and resonance Raman spectra reveal multiple coordination states for H175G/Im which can be correlated with the crystal structures to assign the following heme environments: H175G/H₂O/H₂O, H175G/Im_d/phosphate_c, H175G/Im_d/H₂O_c, H175G/Im_c/H₂O_d, and H175G/Im_c/OH[−]_c, where H175G/X/Y defines the proximal species as X and the distal species as Y and c and d subscripts refer, where known, to the coordinated and dissociated states, respectively. Resonance Raman data for reduced H175G/Im show two substates for heme-coordinated Im differing in the strength of their hydrogen bond to Asp-235, in a fashion similar to WT CCP. NO binding to ferrous H175G/Im results in dissociation of Im from the heme but not from the cavity, while no dissociation is observed for WT CCP, indicating that steric tethering may, in part, control NO-induced dissociation of trans ligands. H175G/Im forms an oxidized compound I state with two distinct radical species, each with a dramatically different anisotropy and spin relaxation from that of the Trp-191 radical of WT CCP. It is suggested that these signals arise from alternate conformations of Trp191 having different degrees of exchange coupling to the ferryl heme, possibly mediated by the conformational heterogeneity of Im within the H175G cavity. The kinetics of the reaction of H175G/Im with H₂O₂ are multiphasic, also reflecting the multiple coordination states of Im. The rate of the fastest phase is essentially identical to that of WT CCP, indicating that the H175G/Im_c/H₂O_d state is fully reactive with peroxide. However, the overall rate of enzyme turnover using cytochrome *c* as a substrate is <5% of WT and is unaffected by Im coordination. In summary, Im coordination to H175G results in a number of conformers, one of which is structurally and spectroscopically very similar to WT CCP. However, while this form is fully reactive with peroxide, the reaction with cytochrome *c* remains inefficient, perhaps implicating the altered Trp-191 radical species.

Recent studies have shown that the axial histidine ligand in several heme proteins can be deleted and replaced by exogenous small ligands to generate a range of novel heme protein complexes (1–16). These results pose questions at a new level of detail about how heme coordination dictates function, and how the protein environment enforces or modulates the properties of the heme–ligand complex. Initial reports of the substitution of imidazole for histidine in

myoglobin (Mb)¹ (1) and cytochrome *c* peroxidase (CCP) (2) provided crystallographic observations of imidazole coordination within the cavity formed by deletion of the native histidine. Spectroscopic data showed that in the absence of added ligands, the ferric state of both H93G Mb (14) and H175G CCP (9) exist as mixtures of water- and hydroxide-coordinated species. Subsequent studies have provided spectroscopic, kinetic, and thermodynamic parameters for binding of various substituted imidazole (4–7, 15–17) and thiolate (12, 18) ligands to the H93G mutant of

[†] This work was supported in part by grants from the National Institutes of Health (GM41049 and GM48495 to D.B.G. and GM34468 to T.M.L.) and by a Wellcome Trust Prize International Research Fellowship to J.H.

* To whom correspondence should be addressed. Phone: (858) 784-9892. Fax: (858) 784-2857. E-mail: dbg@scripps.edu.

[‡] The Scripps Research Institute.

[§] Current address: Medical Research Council, Dunn Human Nutrition Unit, Hills Rd., Cambridge, CB2 2XY, U.K.

^{||} Current address: Pharmacia Corporation, Department of Protein Science, 301 Henrietta St., Kalamazoo, MI 49001.

[⊥] Oregon Graduate Institute of Science and Technology.

¹ Abbreviations: CCP, cytochrome *c* peroxidase; CCP(MKT), cytochrome *c* peroxidase produced by expression in *Escherichia coli* containing Met-Lys-Thr at the N-terminus, Ile at position 53, and Gly at position 152; H175G, mutant in which His-175 is replaced by Gly; H175G/X_{c/d}/Y_{c/d}, state in which ligand X occupies the proximal heme cavity, ligand Y occupies the distal heme cavity, and these are either coordinated (c) to or dissociated (d) from the heme iron; WT, wild-type CCP; cyt *c*, cytochrome *c*; Mb, myoglobin; EPR, electron paramagnetic resonance; RR, resonance Raman; Im, imidazole.

myoglobin (Mb). Finally, partial rescue of functional activity by Im has been reported in the horseradish peroxidase H170A mutant (8). Thus, exogenous ligand replacements are possible in each of the archetypal globin and peroxidase structures, allowing interesting comparisons to be made with respect to the proposed roles of the axial ligand in these different proteins.

Although the "push-pull" concept has been widely regarded as the pivotal difference in reactivity between globins and heme enzymes (19), the relative importance of the proximal-push has recently come under question. Heme-containing globins, such as Mb, form stable ferrous-dioxygen complexes, and the ferric forms are either unreactive, or react only slowly with peroxide (20). In contrast, most heme enzymes, such as peroxidases, P₄₅₀S and nitric oxide synthases (NOS), form reactive ferric-peroxy and ferrous-dioxygen complexes that readily undergo heterolytic cleavage of the O-O bond to generate oxidized ferryl heme species (21). In peroxidases, a histidine-arginine pair in the distal heme cavity produces a distal-pull effect, providing acid-base and electrostatic assistance for the heterolytic O-O bond cleavage step (19, 21). In support of this mechanism, mutations of these distal residues in peroxidases have large and specific effects on peroxy bond cleavage (22). In addition, repositioning of the distal histidine in Mb, not normally oriented properly for this role, has provided Mb variants with increased reactivity toward peroxide (16, 23, 24).

On the other hand, a proximal-push effect, arising from an electron donating proximal heme ligand, has been proposed to stabilize the oxidized ferryl intermediates of many heme enzymes (19, 21, 25-27). For thiolate coordinated enzymes, such as P₄₅₀ and NOS, the absence of residues capable of providing the distal-pull effect has led to a widespread acceptance of the importance of proximal push in these systems (19, 21, 28). Peroxidases contain an axial histidine heme ligand strongly hydrogen bonded to an aspartate side chain; this interaction may partially deprotonate the histidine and thus produce a strong imidazolate-like ligand (19). In CCP, spectroscopic and redox potential studies have indicated that disruption of the Asp-His hydrogen bond has significant effects on the strength of the axial ligand (27-30). However, several recent results appear to be inconsistent with the proximal push concept in CCP (31). For example, it was shown that the axial histidine of CCP can be replaced by glutamate or glutamine without significantly impairing function, implying that the delicately balanced Asp-His ligand was not strictly required for function (32, 33). In addition, studies on H93G Mb, in which the basicity of the axial imidazole ligand was varied, showed changes in reactivity only weakly correlated with the pK_a of the imidazole (16). Finally, a recent report has even suggested that the axial cysteine ligand of chloroperoxidase can be replaced by histidine without loss of function (34), although this has not been verified. These results clearly show, that while axial ligand identity may modulate functional properties or help in maintaining an active coordination state, it is not strictly required for activity, thus reopening many old issues about exactly what role the axial ligand does take in these enzymes.

The preceding paper in this issue (35) describes a number of crystal structures of the imidazole-bound H175G mutant

that provide a firm foundation for interpretation of the spectroscopic and functional properties of this ligand deficient mutant. We use the nomenclature H175G/X_{c/d}/Y_{c/d} to represent the state in which ligand X occupies the proximal heme cavity, ligand Y occupies the distal heme cavity, and these are either coordinated (c) to or dissociated (d) from the heme iron. A more simplified notation H175G/X refers to the protein in the presence of ligand X where the occupation and coordination are unspecified. With insights provided by crystal structures characterizing the phosphate bound state and the pH dependence of axial imidazole coordination, the spectroscopic and functional data can now be rationalized and placed in context of the active site structure. Most importantly, the contrasting properties of the H93G Mb and H175G CCP axial ligand replacements provide the opportunity to inquire, at a new level of detail, into the intrinsic differences in their axial ligand function.

EXPERIMENTAL METHODS

Protein Expression and Purification. Expression of CCP-(MKT) and the H175G mutant from *Escherichia coli* was carried out as described previously (2). All samples of H175G, unless specifically noted, were prepared in the phosphate-free form as described in the previous paper in this issue (35). Protein was stored frozen at 77 K as a crystal suspension in distilled water and prepared for spectroscopic studies by removing the supernatant and dissolving the crystals in a minimal volume of 500 mM MES at the appropriate pH, centrifuged to removed insoluble material and then diluted into the final buffer conditions. Imidazole ligands were added to the specified concentration from pH adjusted stock solutions.

UV-vis Spectroscopy, Binding, and Kinetic Measurements. UV-vis absorption spectra were collected at 20 °C using a Hewlett-Packard 8453 diode-array spectrometer. Imidazole binding constants were determined by recording spectra on separate aliquots of H175G as a function of imidazole concentration in 100 mM MES buffer, rather than successive titration of a protein with imidazole. This was necessary due to the relatively long times required under some conditions (ca. 10 min) to reach equilibration. Each sample was monitored for approach to equilibrium in the cuvette before the spectrum was recorded. Care was taken to record a whole series of spectra using the same protein stock, thus establishing the same protein concentration in each spectrum and allowing direct comparison. Dissociation constants and cooperativity were evaluated using Scatchard and Hill plots. Scatchard plots were linear over the measured range and a single set of isosbestic points was observed (for example, at 393, 564, and 592 nm for H175G + Im, pH 6). Kinetic spectrometric measurements for the peroxide reaction were conducted using an OLIS RSM-1000 rapid scanning stopped-flow spectrometer. Solutions of protein (final concentration 2-5 μM) were prepared in 100 mM MES buffer at pH 6 and equilibrated to temperature in the spectrometer prior to reaction with a second solution of H₂O₂ (0-20 μM). Both solutions contained the same imidazole concentration. Steady-state kinetics of cytochrome *c* oxidation were measured at 20 °C in buffer containing 100 mM MES (pH 6), and 20 mM imidazole where specified. Reactions contained 25 μM of prerduced horse heart cytochrome *c*, 250 pM enzyme, and varying concentrations of H₂O₂. Under these

conditions, initial rates were linear over at least 10 s and the oxidation of cytochrome *c*, monitored at 550 nm, was used to calculate the rate of enzyme turnover. Where possible an Eadie–Hofstee plot was used to calculate an effective k_{cat} , the rate constant under limiting peroxide concentration, measured with 25 μM cytochrome *c*.

Resonance Raman Spectroscopy. RR spectra were obtained on a custom McPherson 2061/207 spectrograph set at 0.67 m with a 2400 groove grating and equipped with a Princeton Instruments (LN-1100PB) liquid-N₂-cooled CCD detector. Kaiser Optical supernotch filters were used to attenuate Rayleigh scattering. Excitation sources consisted of an Innova 302 krypton laser (413 nm) and a Liconix 4240NB helium/cadmium laser (442 nm). Frequencies were calibrated relative to indene and CCl₄ standards and are accurate to $\pm 1\text{ cm}^{-1}$. The integrity of the Raman samples before and after laser illumination was confirmed by direct monitoring of their UV–vis spectra in the Raman capillaries.

Electron Paramagnetic Resonance. EPR spectra were recorded on a Bruker ESP X-band spectrometer using a TE102 rectangular cavity maintained at low temperature by an Air Products LTR-3 liquid helium cryostat; sample temperature was measured with a calibrated GaAs diode. Power levels were determined to be below microwave saturation, and 100 kHz field modulation amplitudes chosen to avoid signal distortion and rapid-passage effects. Samples of ferric enzyme contained 50% glycerol to suppress freezing induced conversion to a low-spin state (36). Compound I was produced by adding H₂O₂ from a concentrated stock solution directly to a 4 mm quartz EPR tube containing ferric enzyme without glycerol, followed by mixing and freezing to 77 K within 15 s. Samples of the ferrous-NO complex were also prepared directly in EPR tubes in the absence of glycerol by reduction with a 2-fold excess of sodium dithionite, followed by addition of a small aliquot of saturated NO solution (prepared by bubbling NO through an oxygen free solution) before freezing in liquid nitrogen. All samples were kept strictly anaerobic throughout by use of a glovebox with a N₂ atmosphere. Control samples reduced in this fashion, but without the addition of NO, displayed little or no signal from ferric heme; further, identical ferrous-NO samples gave UV–vis spectra consistent with the desired conversion when observed using a 1 mm path-length cuvette.

RESULTS

UV–Vis Spectroscopy and Imidazole Binding. The effects of imidazole binding on the UV–vis spectra of H175G CCP have been reexamined following the crystallographic observations (see preceding paper in this issue) that imidazole coordination is pH dependent, and phosphate can coordinate to the iron on the distal heme face of H175G. As shown in Figure 1, in the absence of Im and phosphate, H175G exhibits a broad Soret band with a maximum of 390 nm, which is pH independent between pH 5 and 7 (data not shown). This is in contrast to the pH dependence previously reported for H175G in phosphate buffers (9), where the 390 nm form at pH 7 converted to a form with a sharper Soret peak at 408 nm at pH 5.

A number of additional coordination states can be detected by UV–vis spectroscopy for H175G in the presence of imidazole. Addition of 15 mM Im to H175G in the absence

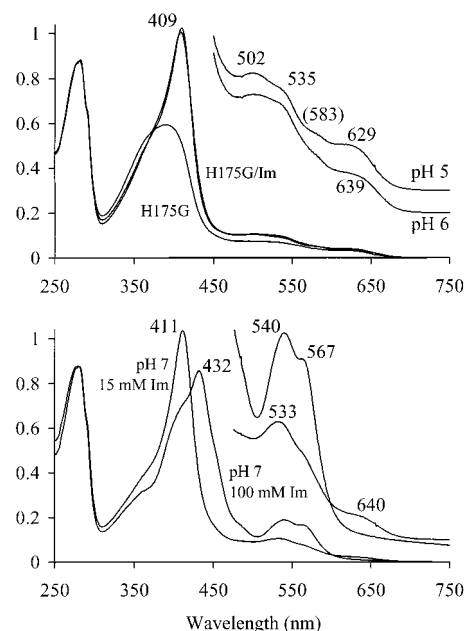


FIGURE 1: UV–vis spectra of imidazole-free and imidazole-bound H175G as a function of pH. The top panel shows spectra at pH 6 in the absence of imidazole, at pH 5 in the presence of 15 mM imidazole and at pH 6 in the presence of 10 mM imidazole. In the bottom panel, spectra were recorded at pH 7 in the presence of 15 mM imidazole. This spectrum is overlaid on that at higher imidazole concentration (100 mM imidazole, pH 7) where the heme appears to be removed from the protein. In all cases solutions contained 10 μM H175G and 100 mM MES buffer and spectra were recorded at equilibrium at 20 °C.

of phosphate causes a conversion of the UV–vis spectra with a single set of inflection points to a high-spin species with a sharp Soret maximum at 409 nm between pH 5 and 6, shifting to 411 nm at pH 7 (Figure 1). The pH-dependent changes are more evident in the visible region, where the charge-transfer band at 629 nm shifts to 639 nm as the pH is raised from 5 to 6. At pH 7, H175G in 15 mM Im converts partially to a low-spin state as evidenced by the 411 nm Soret maximum and the weak $\alpha\beta$ bands observed at 533 and 568 nm (sh). Finally, as the Im concentration is raised to 100 mM at pH 7, the spectrum shifts dramatically to that with a Soret maximum of 432 nm and with prominent $\alpha\beta$ bands at 540 and 567 nm. This spectrum is unlike that of low-spin heme proteins, but is essentially identical to that of free heme in imidazole containing buffer, indicating that the heme is removed from H175G by high concentrations of Im at pH 7.

Equilibrium dissociation constants for Im binding to H175G were found to be pH dependent, reflecting imidazole protonation as well as the final coordination state of the complex. UV–vis spectra collected as a function of total Im concentration were fit to a single binding equilibrium model as described in the Experimental Methods and the overall dissociation constants (expressed in terms of the total imidazole concentration, $[\text{Im}] = [\text{H}_2\text{Im}^+] + [\text{HIm}]$) are $K_d^{\text{tot},5} = 1.5\text{ mM}$, $K_d^{\text{tot},6} = 0.5\text{ mM}$, and $K_d^{\text{tot},7} = 9\text{ mM}$ at pH 5, 6, and 7, respectively. The values determined at pH 7 are only approximate as binding was partially obscured by the above-noted loss of heme at high [Im]. Thus, as the pH is raised and the complex converts from the high- to low-spin state, imidazole binding becomes dramatically weaker. This is despite the higher relative concentration of unprotonated

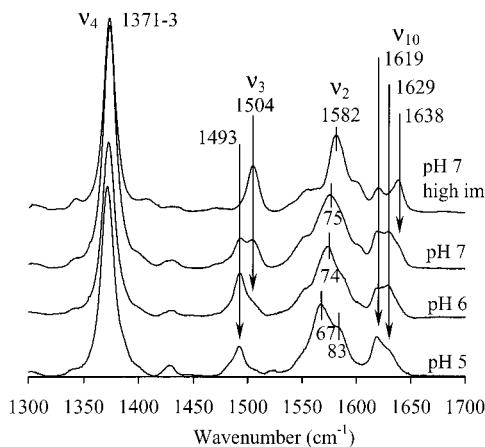


FIGURE 2: High-frequency RR spectra of H175G in 200 mM MES buffer at pH 5 with 15 mM imidazole, at pH 6 with 10 mM imidazole, and at pH 7 with 15 and 50 mM imidazole. Spectra were acquired at room temperature for 2 min by excitation at 413 nm with 5 mW of power.

imidazole at higher pH, which we assume to be the coordinating species.

Resonance Raman Spectroscopy. Resonance Raman scattering was used to further characterize the coordination states of H175G and their dependence on axial ligand, temperature, and solution/crystalline states. Spectra in the high-frequency region for the ferric H175G/Im complex are shown in Figure 2. In the presence of 10–15 mM Im, the protein exhibits a pH-dependent conversion from a 5-coordinate high-spin state at pH 5 ($\nu_3 = 1493 \text{ cm}^{-1}$) to a mixture of 5-coordinate high-spin and 6-coordinate low-spin states ($\nu_3 = 1504 \text{ cm}^{-1}$) at pH 7. This low spin state is distinct from that obtained at 50 mM Im concentration where the heme appears to be removed from the protein. Importantly, RR data collected from H175G crystals suspended in solutions containing 15 mM Im at pH 6 or 7 are essentially identical to the solution spectra of Figure 2 (data not shown). This comparison establishes that the spectroscopic data collected on samples in solution accurately reflect the observed coordination states observed in the crystal structures of these complexes.

Details of the coordination and hydrogen bonding between Asp-235, Im, and heme were obtained by RR scattering of the reduced ferrous protein. In WT CCP, two Fe-histidine stretching modes at 233 and 246 cm^{-1} correspond to states in which the histidine is weakly or strongly hydrogen bonded to Asp235, respectively (26). Resonance Raman data in the low-frequency region for reduced H175G and its imidazole complex at pH 6 are shown in Figure 3. No Fe–Im stretching modes are observed in the absence of Im, and the spectrum is consistent with those of other heme proteins and mutants lacking axial histidine coordination. In the presence of 10 mM Im, two new bands are observed at 230 and 256 cm^{-1} . Confirmation that both of these bands result from Fe–Im vibrations was obtained by comparison of samples containing ^{14}N -imidazole and ^{15}N -imidazole. As shown in Figure 3, the bands at 230 and 256 cm^{-1} both shifted to lower frequency by 1 and 1.5 cm^{-1} , respectively.

Electron Paramagnetic Resonance. Low-temperature EPR was found to be an effective method for distinguishing the variously coordinated forms of H175G. Figure 4 compares the EPR spectra at 7 K for WT CCP, H175G in the absence of exogenous ligands, and for the phosphate and imidazole

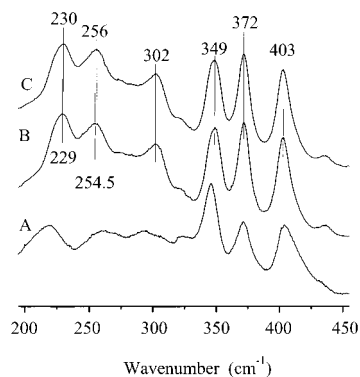


FIGURE 3: Low-frequency RR spectra of dithionite-reduced H175G in 100 mM MES pH 6.0, in the absence of imidazole (A), in 10 mM $^{15}\text{N}_2$ -imidazole (B), and in 10 mM $^{14}\text{N}_2$ -imidazole (C). Spectra were obtained with 442-nm excitation (4 mW) at room temperature, with a total acquisition time of 20 min.

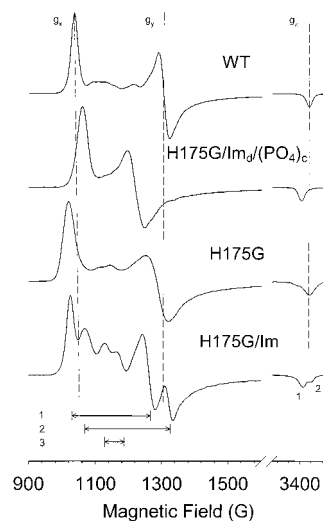


FIGURE 4: Ferric state EPR spectra for H175G as a function of imidazole and phosphate. The fundamental differences in coordination states of H175G are shown for WT CCP in 500 mM MES buffer, 20 mM imidazole; phosphate coordinated H175G (H175G/Im₄/phosphate₃) in 20 mM imidazole, 100 mM phosphate buffer; H175G in 200 mM MES buffer; H175G/Im in 20 mM imidazole, 500 mM MES. For each sample, the pH was 6.0, and glycerol was added to 50% to prevent freezing induced transition to low spin forms. All spectra have been corrected for slight differences in microwave frequency and are reported for a frequency of 9.52 GHz. In all cases, microwave power was 1.0 mW (except H175G: 0.1 mW), and a modulation amplitude of 5 G at 100 kHz, conversion time of 82 ms, and time constant of 328 ms were used. The numbers 1, 2, and 3 designate three separate high-spin ferric heme signals observed in the H175G/Im sample with the indicated splitting between g_x and g_y .

coordinated states. Each of the signals are characteristic of an $S = 5/2$ high-spin ferric heme in a rhombically distorted axial environment with $g_x \approx g_y \approx 6$ and $g_z \approx 2$. WT CCP, H175G and H175G/Im₄/phosphate₃ each show a single, predominant high-spin signal, but can be distinguished from each other by small differences in E/D (rhombicity), line-width, and average g value (Figure 4 and Table 1). The signal for H175G in the absence of exogenous ligands has a somewhat broader line-width, and a larger rhombicity compared with WT CCP, while H175G/Im₄/phosphate₃, which was shown by crystallography to contain a coordinated phosphate and a dissociated Im, exhibits a smaller rhombic distortion compared to WT CCP. It is also noted that both

Table 1: EPR Parameters for the Ferric High-Spin Complexes of H175G

	g_x	g_y	$(g_x + g_y)/2$	E/D^a
WT	6.58	5.21	5.90	0.0285
H175G/Im _d /phosphate _c	6.44	5.59	6.01	0.0177
H175G	6.70	5.27	5.99	0.0298
H175G/Im species 1	6.63	5.40	6.01	0.0256
H175G/Im species 2	6.37	5.23	5.80	0.0238
H175G/Im species 3	6.03			
H175G + 2MeIm	6.50	5.52	6.01	0.0204
H175G + 1MeIm	6.61	5.38	6.00	0.0256
H175G + 4MeIm species 1	6.63			
H175G + 4MeIm species 2	6.49	5.20	5.85	0.0269

^a E/D calculated from $g_x - g_y = 48 (E/D) (59)$.

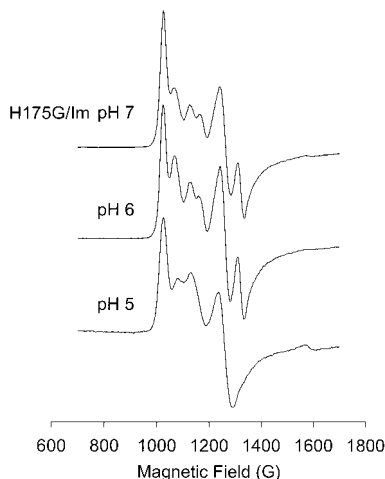


FIGURE 5: pH dependence of the EPR spectra of H175G/Im is shown for samples containing 20 mM imidazole and 500 mM MES buffer adjusted to the indicated pH and 50% glycerol. Sample and EPR conditions are as described in Figure 4.

of these signals have a slightly larger value of $(g_x + g_y)/2 = 6.0$ compared with a value of 5.9 for WT CCP.

In contrast to the Im free forms, a mixture of coordination environments is observed for H175G in the presence of 20 mM Im at pH 6, where at least three high-spin signals appear to contribute to the spectrum (Figure 4). Variation in the relative contribution of these signals with sample pH (Figure 5) allows the assignment of g values to individual species, labeled 1, 2, and 3 at the bottom of Figure 4 and in Table 1. Species 1 and 2 have similar values for E/D , which are intermediate between those of H175G and H175G/Im_d/phosphate_c. Species 3 is a nearly axial species, and it was not possible to determine E/D from the unresolved g_x and g_y components. Species 1 is distinguished from species 2 by differences in $(g_x + g_y)/2$ which are 6.01 and 5.8, respectively. The values of $(g_x + g_y)/2$ shown in Table 1 suggest that signal 1 may result from a heme environment that is similar to that of H175G with $(g_x + g_y)/2 = 5.99$ and signal 2 may correspond to an environment like that of WT CCP with $(g_x + g_y)/2 = 5.9$ (see Table 1). At pH 5, only species 1 and 3 are seen, while species 2 develops as the pH is raised to 6. As the pH is raised further to 7, species 1 and 2 persist along with the appearance of additional low-spin signals (not shown). Finally, a number of methylimidazoles were examined in an attempt to reconstitute the active site in a fully native state. So far, these efforts have met with only limited success except that it has been possible to

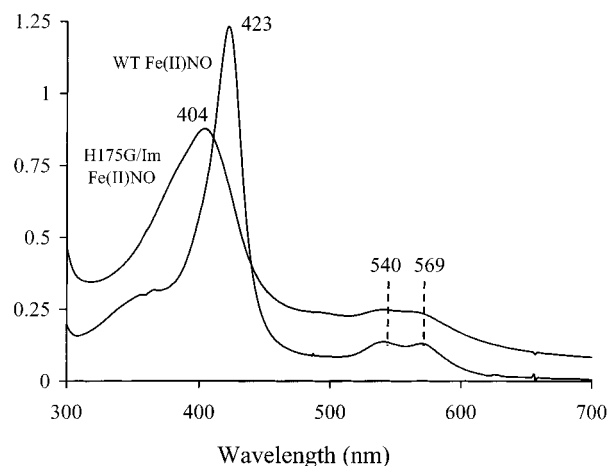


FIGURE 6: UV-vis characteristics of the ferrous NO complexes of WT CCP and H175G/Im. UV-vis samples were prepared by adding small aliquots of a stock NO solution to samples of dithionite-reduced enzyme in a sealed anaerobic cuvette. Saturated NO solutions were made by bubbling NO gas first through a KOH trap and then into anaerobic buffer in a crimp-sealed vial. Samples contained 100–200 mM MES, pH 6 at 20 C, H175G/Im contained additionally 15 mM imidazole.

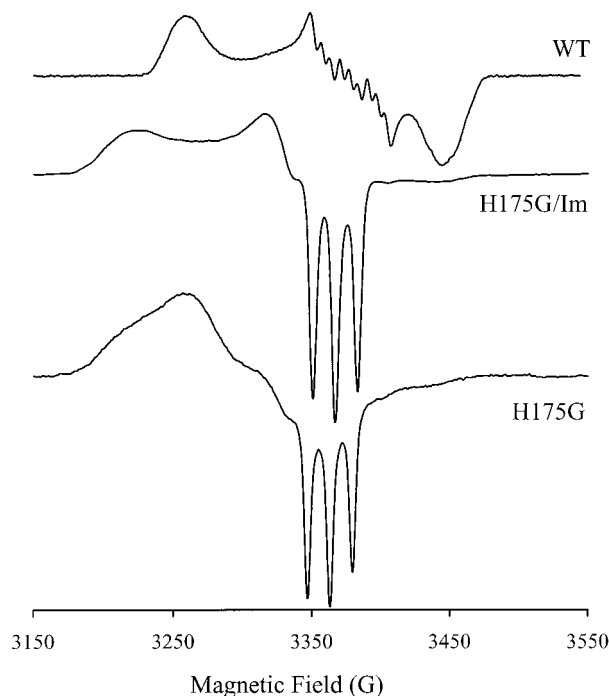


FIGURE 7: EPR spectra for the ferrous-NO complexes of WT CCP, H175G, and H175G/Im. Samples were prepared as described in Figure 6. EPR spectra were collected at 9.52 GHz, 0.1 mW microwave power, 100 MHz field modulation and at 70 K (WT CCP) or 35 K (H175G and H175G/Im).

observe variations in the relative contributions of species similar to 1, 2, and 3 as the position of the methyl substituent is varied.

Ferrous-NO Complexes. The spectroscopic and structural data indicating that the proximal Fe–Im bond of H175G/Im is tenuous and prone to dissociation is augmented by the observation that NO binding to H175G/Im clearly results in full dissociation of any bound Im. UV-vis and EPR spectra of the ferrous-NO complexes of WT CCP and H175G/Im are compared in Figures 6 and 7. The UV-vis spectra clearly indicate different ferrous-NO complexes for the two proteins.

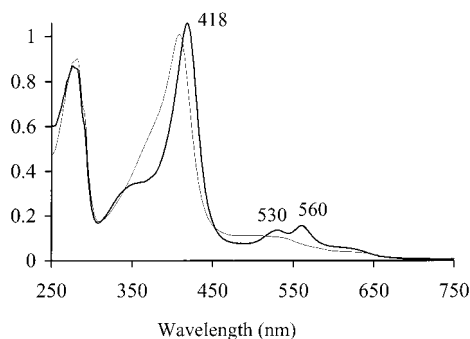


FIGURE 8: UV-vis spectra at 20 °C for 10 μ M H175G/Im (10 mM imidazole, 100 mM MES, pH 6) before (light line) and after (bold line) reaction with a 2-fold excess of H_2O_2 , showing the conversion from Fe(III) to Fe(IV)=O.

The broadened and blue shifted Soret for H175G/Im/NO ($\lambda_{\text{max}} = 404$ nm) compared with WT CCP/NO ($\lambda_{\text{max}} = 423$ nm) are consistent with 5-coordinate and 6-coordinate ferrous nitrosyl complexes, respectively (37). The EPR spectrum of the WT ferrous-NO complex shows the 9-line hyperfine pattern in the g_y region that is characteristic of the $S = 1/2$ spin coupled to two nitrogens (38), clearly indicating that both NO and the proximal His-175 are simultaneously bound. However, the 3-line pattern observed for the H175G/Im ferrous-NO complex shows that only one nitrogen is coupled to the radical, demonstrating that the Im has dissociated from the heme. As shown at the bottom of Figure 7, a somewhat different ferrous-NO complex is observed for H175G in the absence of Im, perhaps indicating that dissociated imidazole is retained in the proximal cavity.

Functional Properties of H175G/Im. The reactivity of H175G CCP toward H_2O_2 is highly dependent on its coordination state. Following our original report of the reaction of H175G/Im with H_2O_2 to produce an unusual compound I state (2), efforts to produce and characterize this state met with only limited success. These difficulties have now been resolved with the identification of phosphate and pH-dependent imidazole coordination to this mutant. Thus, in the presence of both Im and phosphate, H175G is essentially unreactive toward H_2O_2 due to the direct coordination of phosphate within the distal heme cavity. However, as shown in Figure 8, in the absence of phosphate, addition of H_2O_2 to H175G/Im results in complete conversion to a species with an optical spectrum characteristic of the ferryl species ($\text{Fe}^{4+}=\text{O}$). This reaction is dependent on the presence of imidazole. Experiments are most advantageously carried out at pH 6 as a compromise between maximizing the state with imidazole directly coordinated to the heme, while avoiding conversion to a low-spin species. In the presence of 10 mM Im at pH 6, greater than 95% of the protein has Im bound within the cavity, but the heme exists as a mixture of Im coordinated and dissociated states. Under these conditions, reaction with excess H_2O_2 results in the conversion of ferric H175G/Im to the ferryl state via a number of kinetic phases ranging from a few milliseconds to many seconds. The fastest observable phase is on a sufficiently separate time scale to be isolated and fit to a single exponential, giving a pseudo-first-order rate constant which increased linearly with $[\text{H}_2\text{O}_2]$ and was independent of [Im]. As shown in Figure 9 and Table 2, this rapid phase, with a second-order rate of $3.55 \times 10^7 \text{ M}^{-1} \text{ s}^{-1}$, compares

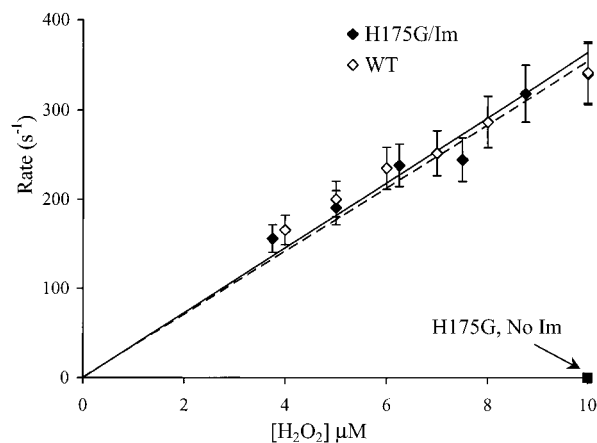


FIGURE 9: Stopped-flow kinetics for the reaction of WT CCP (open diamonds), H175G (closed squares), and H175G/Im (closed diamonds) with peroxide. The pseudo-first-order rate constants for the rapid phase of the reaction are shown as a function of H_2O_2 concentration, along with the linear least-squares fits to give the second-order rate constants of Table 2.

well with the value of $3.64 \times 10^7 \text{ M}^{-1} \text{ s}^{-1}$ observed for WT CCP under the same conditions. In the absence of Im, no corresponding fast phase is observed and, under these conditions, H175G reacts only slowly ($7.33 \times 10^3 \text{ M}^{-1} \text{ s}^{-1}$) with H_2O_2 . Notably, the *rate constant* for the fast phase is independent of [Im], while its *magnitude* is dependent on [Im], as the degree to which the heme is bound with imidazole changes. At > 10 mM Im, the amplitude of the fast phase is of the same order as that for WT CCP, while the amplitude decreases at lower [Im], becoming too small to accurately measure at < 1 mM. The slower phases following this initial burst are complex and nonexponential, and we have been unable at present to obtain a satisfactory quantitative analysis of them.

The steady-state rate of cyt *c* oxidation by H_2O_2 catalyzed by H175G/Im was reexamined to determine if the low values previously reported could have resulted from phosphate inhibition. Our earlier study reported that cyt *c* turnover for H175G was only 4% of that observed for WT CCP and was not stimulated by addition of Im. As shown in Table 2, cyt *c* oxidation by H175G in the absence of phosphate is very similar to the previous values, and the rate is not significantly stimulated by the presence of Im. Thus, despite the fact that the 5-coordinate Im bound form of H175G is fully reactive with H_2O_2 , it is capable of sustaining only 4% of the activity of wild-type CCP with respect to the oxidation of cyt *c*.

Compound I Radical Species. H175G/Im in the compound I state contains two radical species that differ from that of the Trp-191 radical in WT CCP. Figure 10 shows EPR spectra at 7 K for the compound I state of WT CCP and H175G/Im. An EPR signal with an unusual line-shape is observed for H175G/Im that integrates at low power to ~ 0.8 spins/protein molecule and, thus, is likely to represent a stoichiometric radical center (39–42). By examination of its power dependence, it appears that two distinct signals are present that differ in line-shape and signal saturation characteristics. At high power (200 mW), a positive derivative peak at approximately 3390 G and a broad derivative feature at approximately 3550 G is seen. At much lower power (2 μ W) an additional, more isotropic signal near $g = 2$ appears. The high- and low-power spectra shown in Figure

Table 2: Kinetic Parameters for the Reaction of H175G with H₂O₂ and for the Oxidation of Cytochrome *c*

	H175G ^a	H175G/Im ^a	WT	WT + Im
reaction with H ₂ O ₂ (M ⁻¹ s ⁻¹)	7.33 × 10 ³ (0.02%)	3.55 × 10 ⁷ (98%)	3.73 × 10 ⁷ (100%)	3.64 × 10 ⁷ (100%)
steady state cyt <i>c</i> oxidation (s ⁻¹) ^b	~11 (5%)	~31 (4%)	209 (100%)	712 (100%)

^a Second-order rate constant for the fastest observable phase of the reaction. The overall reaction kinetics were multiphasic. ^b Relative rates of cytochrome *c* oxidation expressed as CCP turnovers per second measured at [CCP] = 250 pM, [Cyt *c*] = 25 μM, [H₂O₂] = 250 μM.

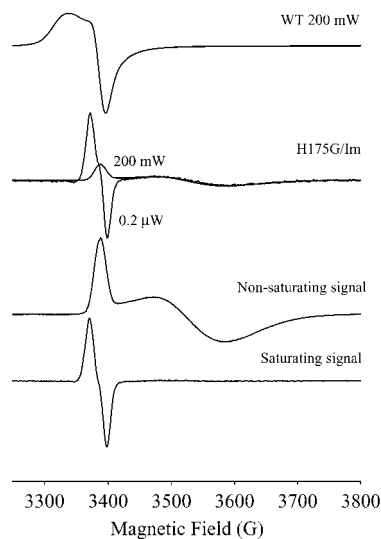


FIGURE 10: EPR properties for the compound I radical species of WT CCP and H175G. Signals are compared for H₂O₂-oxidized samples of WT CCP and H175G in the presence of 20 mM Im. Protein concentration was ~200 μM and a 2-fold excess of H₂O₂ was added immediately before freezing. Spectra for H175G/Im are shown at 200 mW and 0.2 μW microwave power, while the WT CCP spectrum is shown at 200 mW. The intensity of each scan was normalized with respect to protein concentration and receiver gain before plotting. Two distinct signals in the oxidized H175G/Im sample, corresponding to rapidly and slowly relaxing species, are separated by subtraction of the normalized high and low power spectra, assuming that the slowly relaxing species is fully saturated at high power. The nonsaturating signal represents 75% of the total integrated signal amplitude.

10 have been appropriately scaled to demonstrate that the low-power signal appears to be a combination of both signals, as expected. This is most readily seen by comparing the broad feature at about 3550 G. Matching of the signal amplitudes in this way allowed the separation of the two signals by subtraction. These signals are shown in Figure 10 to consist of a 25% contribution from an isotropic signal with a zero crossing at $g = 2.012$, and a 75% contribution from a signal with apparent axial symmetry: $g_{\perp} = 1.940$, $g_{\parallel} = 2.013$. Power saturation curves, shown in Figure 11, verify the distinct assignment of these two signals. The isotropic signal is seen to saturate at about 0.1 mW, whereas the axial signal shows no signs of saturation even at 200 mW, at 7 K.

DISCUSSION

Imidazole Binding and Coordination Environment. The spectroscopic studies of this paper can be combined with the structural information of the preceding paper in this issue (35) to provide a detailed account of imidazole coordination to the proximal ligand cavity mutant (H175G) of CCP. Our results reveal a rich and subtle variation in heme coordination environment that is very sensitive to conditions, such as buffer ion composition and ligand protonation state.

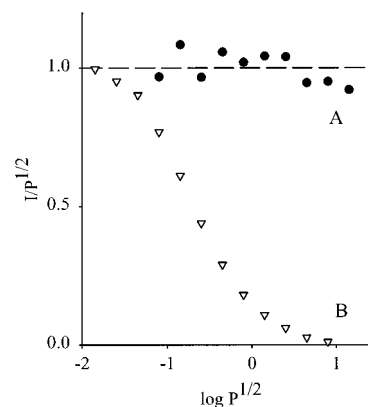


FIGURE 11: Power saturation curves for the two isolated EPR signals of H175G/Im compound I. The signal amplitude normalized by the square root of the microwave power (in mW) is plotted against $\log P^{1/2}$ for the nonsaturating signal (A, filled circles) and the saturating signal (B, open triangles).

The discovery that phosphate binds to the H175G mutant has resolved the somewhat perplexing behavior of this mutant. Earlier reports of imidazole binding to H175G CCP suggested a pH-dependent conversion of H175G from a 5-coordinate water bound form at pH 6 to an iron-hydroxo species at pH 7 (9), to which Im bound to give the 5-coordinate imidazole complex (2). With the observation of phosphate coordination to the heme in the preceding paper in this issue, the earlier results have been revisited to separate the effects of imidazole from phosphate coordination. The results of this work show that the pH dependence of the H175G spectra in the absence of Im is only seen in phosphate buffer and is thus likely to reflect coordination by phosphate, as observed in the crystal structures. As the 390 nm form in the absence of Im and phosphate corresponds to the high pH form in the presence of phosphate, we propose that this form does not have phosphate coordinated. Thus, whereas a hydroxyl is bound at pH 7.0 (9), phosphate coordination occurs at lower pH, and results in a conversion of the Soret band from 390 to 408 nm. In addition, the large rearrangement observed in the distal protein structure associated with phosphate coordination provides comprehension of the rather slow and irreproducible ligand binding experiments that have been observed in our laboratory with this mutant.

The Im binding affinity is highly pH dependent, reflecting the protonation state of the ligand and the final coordination state of the protein. The overall Im binding affinity, expressed in terms of $[Im]_{tot}$, goes through an optimum at pH 6 and is slightly weaker and considerably weaker at pH 5 and 7, respectively ($K_d^{tot,5} = 1.5$ mM, $K_d^{tot,6} = 0.5$ mM, and $K_d^{tot,7} = 9$ mM at pH 5, 6, and 7). The value at pH 7 ($K_d^{tot,7} = 9$ mM) compares favorably with that determined for Im binding to the H93G Mb mutant ($K_d^{tot,7} = 10$ mM) (16), but the pH dependence has not been reported for other histidine heme ligand mutants. A full treatment of the binding equilibrium must account for changes in the pK_a of Im in the environment

of the H175G cavity compared to that in solution and for the intrinsic K_d values for binding of imidazole in its various protonation states to H175G. However, this analysis is further complicated by the conversion to low-spin at higher pH, effectively precluding determination of limiting K_d and pK_a values. In addition, the observed heterogeneous positional shifts of Im within the protein cavity as a function of pH (see preceding paper in this issue) (35), make it difficult to apply an accurate binding model at this time. It is, however, likely that the neutral, monoprotonated form of imidazole is favored within the cavity, as interactions with both the heme and Asp-235 will serve to reduce the pK_a from that ($pK_a = 7.1$) in solution. The significant increase in binding affinity as the pH is raised from 5 to 6 supports these assumptions. Thus, to a first approximation, the binding constants can be corrected to reflect the concentration of the relevant neutral imidazole in solution in order to provide an estimate of its intrinsic affinity for H175G. Under this assumption, the dissociation constants become $K_d^{\text{tot},5} = 12 \mu\text{M}$, $K_d^{\text{tot},6} = 37 \mu\text{M}$, and $K_d^{\text{tot},7} = 4 \text{ mM}$ at pH 5, 6, and 7, respectively. Thus, binding may be considered in terms of two states of the protein: a high-spin state at low pH with $\sim 12 \mu\text{M}$ affinity for neutral Im, and a low-spin species at pH > 7 with a much weaker affinity for Im.

The optical, resonance Raman, and EPR data on H175G provide a detailed picture for the pH-dependent coordination of Im that is consistent with the structures of the preceding paper in this issue (35). No differences were observed in the coordination environment for structures obtained at room temperature and 100 K. In addition, resonance Raman scattering shows that the coordination environment of H17G-Im does not differ between solution and crystalline states. Thus, the spectroscopic and crystallographic data can be effectively cross-correlated. The structures of the preceding paper show a pH-dependent shift in the position of Im bound within the cavity, so that Im is dissociated from the heme at pH 5, but becomes coordinated at pH 7. As the RR data suggest a 5-coordinate high-spin form at pH 5, this indicates that a water molecule, unresolved in the crystal structure, must be bound to the iron on the distal heme face when Im dissociates. At pH 7, the Raman data show a mixture of 5-coordinate high-spin and 6-coordinate low-spin species. The 5-coordinate form thus represents a state with the proximal Im bound and the distal water dissociated from the heme. These multiple coordination modes are also evident in the EPR spectra of the ferric complexes, where as many as three high-spin and at least one low-spin species are observed. From the pH dependence of these forms, the signals referred to as species 1 and 2 appear to correspond to Im in the iron-dissociated and iron-coordinated states, respectively. Finally, we note that the tendency of H175G to exist in multiple high-spin states is similar to, but more dramatic than that of WT CCP. The important observation, however, is that these states are distinct from those of WT, with variations in both the rhombicity parameter (E/D) and $(g_x + g_y)/2$ (Table 1, Figure 4), indicating that they reflect the slightly different coordination contributed by Im as opposed to the natural histidine. Changes in E/D arising from small alterations in g anisotropy are common, while the variation of $(g_x + g_y)$ from the spin-only value of 6.0, as seen also in WT CCP, imply changes in the spin-orbit

coupling, perhaps as a result of the sensitivity of d orbital hybridization on heme planarity and symmetry.

The unstable character of the Fe-Im bond in H175G/Im indicated by these studies is reflected in a clear difference between the ferrous nitrosyl complexes of H175G/Im and WT CCP. For H175G/Im/NO, the EPR data show that the Im is clearly dissociated from the heme (H175G/Im_d/NO_c), while for WT CCP the axial histidine is retained to form a 6-coordinate ferrous nitrosyl complex (WT CCP/His_c/NO_c). The Raman data show that Im is coordinated to the heme in the ferrous protein before addition of NO and thus NO induces the Im dissociation via its known negative trans effect (6). However, even though NO results in Im dissociation, the ferrous-NO complexes are different in the presence and absence of Im, indicating that Im dissociates from the iron, but does not leave the proximal cavity. The fact that the axial histidine is not dissociated from WT CCP indicates that either steric restriction of its movement by the covalent tether or differences in its intrinsic bond strength due to the electronic effects of hydrogen bonding may be important. These results have potential relevance to guanylate cyclase, where NO induced dissociation of the proximal histidine has become widely recognized as a signaling mechanism (43, 44). Further studies of NO induced ligand dissociation in this tethered and untethered system may provide an improved understanding of the effects of steric, electronic and energetic properties of a ligand on NO induced signaling.

Hydrogen Bonding of Bound Im. Variation of the Fe-His stretching frequency ($\nu_{\text{Fe-His}} = 200\text{--}250 \text{ cm}^{-1}$) in heme proteins is known to correlate with the proximal hydrogen-bonding environment (26). In fact, two Fe-Im stretching modes are observed for WT CCP at 233 and 246 cm^{-1} that have been proposed to arise from the histidine proton in a double potential well with the proton residing primarily on His-175 or Asp-235 (29). Destruction of this hydrogen bond by mutagenesis results in a shift to $\nu_{\text{Fe-His}} = 205 \text{ cm}^{-1}$.

The resonance Raman data can be used to establish that Im coordinated to ferrous H175G is present in two hydrogen-bonding conformations with Asp-235, much like that of WT CCP. Substitution of imidazole for His-175 is expected to have several complex effects on $\nu_{\text{Fe-Im}}$, even if the interactions between Im and Asp-235 are unchanged. With a lower effective mass than histidine, $\nu_{\text{Fe-Im}}$ is expected to occur at higher frequency. However, additional effects arising from changes in mechanical tethering to the protein and small changes in the orientation and tilt of the imidazole ring with respect to the heme (45) make quantitative predictions of $\nu_{\text{Fe-Im}}$ difficult. Nevertheless, in other proteins that have weakly hydrogen-bonded histidines, such as Mb and HO, replacement of histidine with imidazole results in $\nu_{\text{Fe-Im}} = 228\text{--}230 \text{ cm}^{-1}$ (5, 8, 46, 47). In these cases, it is likely that Im forms an unrestrained coordination to the heme iron and is weakly hydrogen bonded. This corresponds well with the 230 cm^{-1} band in H175G/Im and this band is therefore assigned to a weakly hydrogen bonded conformation. Evidence that the second low-frequency band at 256 cm^{-1} also arises from a $\nu_{\text{Fe-Im}}$ mode is obtained from the ^{15}N isotope sensitivity of both $\nu_{\text{Fe-Im}}$ bands. From a simple two-body model, the predicted isotope shifts for the two bands (-1.5 and -1.7 cm^{-1}) are very close to those observed (-1 and -1.5 cm^{-1}). While it is possible that the isotope shift of both bands could arise from coupling of a single Fe-Im

stretch with an out-of-plane heme mode, in this case, the isotope shift would be shared between both coupled modes. As the sum of the observed shifts (-2.5 cm^{-1}) is larger than either predicted shift, this effectively rules out the coupled mode hypothesis as the source of the isotope sensitivity of both bands. Thus, two important conclusions about the ability of imidazole to substitute for His-175 in CCP can be made. First, as with WT CCP, ferrous H175G/Im exists in two imidazole-coordinated conformations that differ in their degree of hydrogen bonding to Asp-235. Second, while distinct coordination differences are observed in the ferric state between WT CCP and H175G/Im, the ferrous forms of these proteins appear quite similar.

Im Rescue of H₂O₂ Reactivity but Not Turnover. The kinetic data presented in this work show that H175G in the Im coordinated conformation fully regains its ability to react with H₂O₂, while the steady-state oxidation of cytochrome *c* remains inefficient. Chemical rescue of functional properties in cavity mutants by complementary small molecules has been observed in a number of enzymes (48–52), including heme proteins (8, 46, 53), and remarkably, it has been observed that His-175 can be replaced with Glu or Gln to give an enzyme with high rates of steady-state cyt *c* oxidation (32, 33, 54). Our results on H175G/Im allow a further conclusion about the operation of the proximal push effect in CCP. The peroxide reactivity of H175G is restored under conditions where Im is bound to the iron. However, the preceding paper in this issue indicates that this state has a somewhat weaker hydrogen bond to Asp-235. Thus, while Asp-235 cannot be replaced without impairing reactivity (27), the hydrogen bond it makes with the axial imidazole can be modulated considerably without serious effects on the peroxide cleavage step.

It remains perplexing that despite the ability of Im to functionally rescue peroxide reactivity in H175G, the oxidation of cyt *c* is still significantly impaired. This result strongly indicates that the major defect with H175G/Im is not with the axial ligand facilitating peroxide heterolysis. It is possible that the enzymatic turnover is limited by some unresolved difficulty in regenerating the active 5-coordinate Im complex after formation of compound I and its reduction to the ferric state by cyt *c*. However, it is more likely that the ability of ferryl enzyme to oxidize cyt *c* is impaired. Indeed, the unusual EPR properties of the compound I radical for H175G/Im support the notion that the properties of this electron-transfer intermediate have been altered.

An Unusual Compound I Radical. Two unique EPR signals are observed for the H₂O₂ reaction product (compound I) of H175G/Im that are proposed to result from forms of Trp-191 with different degrees of exchange coupling with the ferryl heme. The compound I state of WT CCP consists of a ferryl (Fe⁴⁺=O) heme and a cation radical localized on Trp-191 (40). The EPR signal of this radical is only observable at <30 K as a result of rapid spin–lattice relaxation modulated by an exchange interaction (*J*) between the *S* = 1/2 radical and the ferryl heme (39). The broad, complex line-shape has been proposed to result from conformational distribution of the exchange coupling (41, 42). The absolute value of *J* is small, so that conformational heterogeneity can result in a distribution in which *J* ranges from *J* > 0 (ferromagnetic coupling) to *J* < 0 (anti-ferromagnetic coupling). Thus, according to this model, the

line-shape of the Trp-191 radical EPR signal would be exquisitely sensitive to small perturbations in the interactions between Trp-191 and the heme. Indeed, large line-shape changes have been observed in mutants of Asp-235 (27, 55, 56). In the case of H175G/Im, two signals are observed that have dramatically different saturation behavior. The easily saturated signal implies a slow spin–lattice relaxation, thus indicating a radical species that is not coupled to the ferryl heme, consistent with its isotropic line-shape. While this signal may reside on an amino acid other than Trp-191, such as Tyr, such a signal is expected from Trp-191 in the distributed coupling model. For small values of *J*, there will be some subpopulation of centers that have *J* exactly equal to zero, and these centers should show an easily saturated, isotropic radical. Indeed, such a component is always observed in WT CCP. In both WT CCP and in H175G/Im this isotropic component represents a minority species. The majority radical species in H175G/Im, with apparent axial symmetry, is similar to that of WT CCP in that it is difficult to saturate at 7 K, and this is consistent with a significant exchange coupling to the heme. However the symmetry of this signal is reversed with respect to the Trp-191 radical of WT CCP, i.e., $g_{\perp} < g_{\parallel}$. This may indicate an opposite sign for *J*, as compared to the dominant form in the WT enzyme (41). Thus, while the coupling of the Trp-191 radical in WT CCP is predominantly anti-ferromagnetic, that for H175G/Im may be predominantly ferromagnetic. The Trp-191 radical center is widely believed to be a direct intermediate for electron transfer from cyt *c* (57, 58) and while it is unclear whether changes in the exchange coupling would have a direct effect on the function of the enzyme, it is possible that this reflects an altered communication between the heme and radical site. Such a lesion may result in the deficiency that we have proposed for electron transfer from cyt *c*.

ACKNOWLEDGMENT

The authors would also like to thank Dr. Gerard Jensen, Dr. Rabi Musah, and Dr. Melissa Fitzgerald for help and valuable discussions.

REFERENCES

- Barrick, D. (1994) *Biochemistry* 33, 6546–6554.
- McRee, D. E., Jensen, G. M., Fitzgerald, M. M., Siegel, H. A., and Goodin, D. B. (1994) *Proc. Natl. Acad. Sci. U.S.A.* 91, 12847–12851.
- Sun, J., Loehr, T. M., Wilks, A., and Ortiz de Montellano, P. R. (1994) *Biochemistry* 33, 13734–13740.
- DePillis, G. D., Decatur, S. M., Barrick, D., and Boxer, S. G. (1994) *J. Am. Chem. Soc.* 116, 6981–6982.
- Franzen, S., Bohn, B., Poyart, C., DePillis, G., Boxer, S. G., and Martin, J.-L. (1995) *J. Biol. Chem.* 270, 1718–1720.
- Decatur, S. M., Franzen, S., DePillis, G. D., Dyer, R. B., Woodruff, W. H., and Boxer, S. G. (1996) *Biochemistry* 35, 4939–4944.
- Decatur, S. M., DePillis, G. D., and Boxer, S. G. (1996) *Biochemistry* 35, 3925–3932.
- Newmyer, S. L., Sun, J., Loehr, T. M., and Ortiz de Montellano, P. R. (1996) *Biochemistry* 35, 12788–12795.
- Sun, J., Fitzgerald, M. M., Goodin, D. B., and Loehr, T. M. (1997) *J. Am. Chem. Soc.* 119, 2064–2065.
- Barrick, D., Ho, N. T., Simplaceanu, V., Dahlquist, F. W., and Ho, C. (1997) *Nat. Struct. Biol.* 4, 78–83.
- Liu, K., Williams, J., Lee, H., Fitzgerald, M. M., Jensen, G. M., Goodin, D. B., and McDermott, A. E. (1998) *J. Am. Chem. Soc.* 120, 10199–10202.

12. Roach, M. P., Franzen, S., Pang, P. S. H., Boxer, S. G., Woodruff, W. H., and Dawson, J. H. (1997) *J. Inorg. Biochem.* 67, 134.
13. Rector, K. D., Engholm, J. R., Hill, J. R., Myers, D. J., Hu, R., Boxer, S. G., Dlott, D. D., and Fayer, M. D. (1998) *J. Phys. Chem. B* 102, 331–333.
14. Pond, A. E., Roach, M. P., Sono, M., Rux, A. H., Franzen, S., Hu, R., Thomas, M. R., Wilks, A., Dou, Y., Ikeda-Saito, M., de Montellano, P. R. O., Woodruff, W. H., Boxer, S. G., and Dawson, J. H. (1999) *Biochemistry* 38, 7601–7608.
15. Decatur, S. M., Belcher, K. L., Rickert, P. K., Franzen, S., and Boxer, S. G. (1999) *Biochemistry* 38, 11086–11092.
16. Roach, M. P., Ozaki, S., and Watanabe, Y. (2000) *Biochemistry* 39, 1446–1454.
17. Decatur, S. M., and Boxer, S. G. (1995) *Biochemistry* 34, 2122–2129.
18. Roach, M. P., Pond, A. E., Thomas, M. R., Boxer, S. G., and Dawson, J. H. (1999) *J. Am. Chem. Soc.* 121, 12088–12093.
19. Poulos, T. L., and Finzel, B. C. (1984) *Pept. Protein Rev.* 4, 115–171.
20. Ozaki, S., Matsui, T., and Watanabe, Y. (1996) *J. Am. Chem. Soc.* 118, 9784–9785.
21. Dawson, J. H. (1988) *Science* 240, 433–439.
22. Vitello, L. B., Erman, J. E., Miller, M. A., Wang, J., and Kraut, J. (1993) *Biochemistry* 32, 9807–9818.
23. Ozaki, S., Matsui, T., and Watanabe, Y. (1996) *J. Am. Chem. Soc.* 118, 9784–9785.
24. Ozaki, S., Matsui, T., and Watanabe, Y. (1997) *J. Am. Chem. Soc.* 119, 6666–6667.
25. Valentine, J. S., Sheridan, R. P., Allen, L. C., and Kahn, P. C. (1979) *Proc. Natl. Acad. Sci. U.S.A.* 76, 1009–1013.
26. Spiro, T. G., Smulevich, G., and Su, C. (1990) *Biochemistry* 29, 4497–4508.
27. Goodin, D. B., and McRee, D. E. (1993) *Biochemistry* 32, 3313–3324.
28. Ortiz de Montellano, P. R. (1987) *Acc. Chem. Res.* 20, 289–294.
29. Smulevich, G., Mauro, J. M., Fishel, L. A., English, A. M., Kraut, J., and Spiro, T. G. (1988) *Biochemistry* 27, 5477–5485.
30. Sinclair, R., Hallam, S., Chen, M., Chance, B., and Powers, L. (1996) *Biochemistry* 35, 15120–15128.
31. Goodin, D. B. (1996) *J. Biol. Inorg. Chem.* 1, 360–363.
32. Sundaramoorthy, M., Choudhury, K., Edwards, S. L., and Poulos, T. L. (1991) *J. Am. Chem. Soc.* 113, 7755–7757.
33. Choudhury, K., Sundaramoorthy, M., Mauro, J. M., and Poulos, T. L. (1992) *J. Biol. Chem.* 267, 25656–25659.
34. Yi, X., Mroczko, M., Manoj, K. M., Wang, X., and Hager, L. P. (1999) *Proc. Natl. Acad. Sci. U.S.A.* 96, 12412–12417.
35. Hirst, J., Wilcox, S. K., Williams, P. A., Blankenship, J., McRee, D. E., and Goodin, D. B. (2001) *Biochemistry* 40, 1265–1273.
36. Hori, H., and Yonetani, T. (1985) *J. Biol. Chem.* 260, 349–355.
37. Scheidt, W. R., and Ellison, M. K. (1999) *Acc. Chem. Res.* 32, 350–359.
38. Yonetani, T., Yamamoto, H., Erman, J. E., Leigh, J. S. J., and Reed, G. H. (1972) *J. Biol. Chem.* 247, 2447–2455.
39. Hoffman, B. M., Roberts, J. E., Kang, C. H., and E., M. (1981) *J. Biol. Chem.* 256, 6556–6564.
40. Sivaraja, M., Goodin, D. B., Smith, M., and Hoffman, B. M. (1989) *Science* 245, 738–740.
41. Houseman, A. L. P., Doan, P. E., Goodin, D. B., and Hoffman, B. M. (1993) *Biochemistry* 32, 4430–4443.
42. Huyett, J. E., Doan, P. E., Gurbiel, R., Houseman, A. L. P., Sivaraja, M., Goodin, D. B., and Hoffman, B. M. (1995) *J. Am. Chem. Soc.* 117, 9033–9041.
43. Denninger, J. W., and Marletta, M. A. (1999) *Biochim. Biophys. Acta* 1411, 334–350.
44. Burstyn, J. N., Yu, A. E., Dierks, E. A., Hawkins, B. K., and Dawson, J. H. (1995) *Biochemistry* 34, 5896–5903.
45. Othman, S., Richaud, P., Vermeglio, A., and Desbois, A. (1996) *Biochemistry* 35, 9224–9234.
46. Wilks, A., Sun, J., Loehr, T. M., and Ortiz de Montellano, P. R. (1995) *J. Am. Chem. Soc.* 117, 2925–2926.
47. Wilks, A., and Moënne-Loccoz, P. (2000) *J. Biol. Chem.* 275, 11686–11692.
48. Denblaauwen, T., and Canters, G. W. (1993) *J. Am. Chem. Soc.* 115, 1121–1129.
49. Toney, M. D., and Kirsch, J. F. (1989) *Science* 243, 1485–1488.
50. Rynkiewicz, M. J., and Seaton, B. A. (1996) *Biochemistry* 35, 16174–16179.
51. Phillips, M. A., Hedstrom, L., and Rutter, W. J. (1992) *Protein Sci.* 1, 517–521.
52. Boehlein, S. K., Walworth, E. S., Richards, N. G. J., and Schuster, S. M. (1997) *J. Biol. Chem.* 272, 12384–12392.
53. Newmyer, S. L., and Ortiz de Montellano, P. R. (1996) *J. Biol. Chem.* 271, 14891–14896.
54. Choudhury, K., Sundaramoorthy, M., Hickman, A., Yonetani, T., Woehl, E., Dunn, M. F., and Poulos, T. L. (1994) *J. Biol. Chem.* 269, 20239–20249.
55. Scholes, C. P., Liu, Y., Fishel, L. A., Farnum, M. F., Mauro, J. M., and Kraut, J. (1989) *Isr. J. Chem.* 29, 85–92.
56. Fishel, L. A., Farnum, M. F., Mauro, J. M., Miller, M. A., Kraut, J., Liu, Y. J., Tan, X. L., and Scholes, C. P. (1991) *Biochemistry* 30, 1986–1996.
57. Millett, F., Miller, M. A., Geren, L., and Durham, B. (1995) *J. Bioenerg. Biomembr.* 27, 341–351.
58. Miller, M. A., Vitello, L., and Erman, J. E. (1995) *Biochemistry* 34, 12048–12058.
59. Slappendel, S., Veldink, G. A., Vleighbart, J. F. G., Aasa, R., and Malmström, B. (1981) *Biochim. Biophys. Acta* 667, 77–86.

BI002090Q